Internal flow characteristics of Spill-return pressure-swirl atomizers

Milan Maly*[1], Marcel Sapik[1], Ondrej Cejpek[1], Frantisek Lizal[1], Vladimir Ondracek[2], Miroslav Jicha[1] and Jan Jedelsky[1]
[1]Brno University of Technology, Technicka 2, 616 69 Brno, Czech Republic
[2]PBS Velka Bites, a. s., Vlkovska 279, 595 01 Velka Bites, Czech Republic
*Corresponding author: milan.maly@vutbr.cz

Abstract
The spray produced by pressure-swirl atomizers strongly depends on the character of their internal flow. Flow field inside a swirl chamber of small pressure-swirl spill-return atomizers was examined using high-speed imaging with image post processing using an in-house Matlab code. The dimensions of the production atomizers did not allow direct visualization of their internal flow, so a scaled modular, transparent Plexiglas model was used. Its flow characteristics were matched with the originally sized atomizer using dimensionless numbers (Reynolds, Swirl, Froude numbers). The test conditions were limited to the inlet overpressure of 5 kPa and spill-to-feed ratio, *SFR* = 0–0.75. Various spill-return configurations were compared in terms of the spatial and temporal behaviour of the internal air-core, and liquid sheet thickness and its perturbations. The only difference among the tested configurations was the geometrical arrangement of the spill-line (SL) orifice through which the liquid is spilled away. The results show that the presence of the SL orifice affects the internal flow characteristics even when the SL is closed. An axially placed SL orifice causes a decay of the internal air-core. The off-axial SL orifices stabilize the air-core, which is vital for regular formation of the liquid sheet and high-quality spray. However, the turn-down ratio and spray stability were found to be dependent on the distance of the SL orifices from the swirl chamber centreline. The results allow to determine the optimum SL configuration for given application.

Keywords
Internal flow, spill-return, air-core, liquid sheet.

Introduction

Spill-return atomizers are enhanced version of the Simplex atomizers, by means of addition of a passage in a rear wall of the swirl chamber. The liquid, injected to the swirl chamber via tangential ports, is divided into two streams there, one is discharged outside and atomized while the second is spilled away through the spill-line passage. The liquid can be supplied into the swirl chamber under high inlet pressure, p_l, and the injection flow rate is consequently regulated by changing the spill flow rate, which allows to keep the swirl momentum high for wide range of injection flow rates, $\dot{m}_{inj}$. The $\dot{m}_{inj}$ of the Simplex atomizer changes with square root of p_l. Therefore, two times decrease in $\dot{m}_{inj}$ requires fourfold decrease in the p_l, which affects droplet sizes dramatically. The operating regime of spill-return atomizer is typically characterised by a bypass ratio or spill-to-feed ratio, *SFR*. This is a ratio of a spilled flow rate, $\dot{m}_s$, to a pumped flow rate, $\dot{m}_p$ and can reach values from *SFR* = 0, where all the liquid is injected and the atomizer operates in a Simplex mode to *SFR* = 1, where all the liquid is spilled away.
Both the Simplex and spill-return atomizers typically discharge a liquid sheet in form of a hollow cone [1]. The parameters of the liquid sheet, such as liquid sheet thickness, *t*, velocity and perturbations are related to the internal flow characteristics. Centrifugal motion inside the swirl chamber generates an internal air-core due to a low-pressure zone along the swirl chamber centreline. The air from surrounding atmosphere is sucked into this zone through the exit orifice and forms the air-core. The diameter of the air-core defines *t* since the air-core blocks a part of the exit orifice. Moreover, the air-core fluctuations and instabilities affect the liquid sheet perturbations and stability [2] and consequently may change the liquid sheet breakup length. Better stability of the liquid sheet prolongs the breakup distance [3]. From a simple geometrical consideration, where the liquid sheet is considered as the hollow-cone, the longer breakup length results in thinner liquid sheet at the breakup position. Therefore, the generated ligaments are smaller and so the final droplets [4]. Also, the breakup mode can change the ligaments size. The long and short wave breakup was observed in [5] in dependence on liquid sheet gas Weber number, We_g, which reaches a critical value of We_g = 27/16, where a transition from the long to the short wave breakup mode was observed. The long wave breakup produces longer breakup length and tends to create smaller ligaments and droplets. This was confirmed in our previous work [4].
The SL orifice can have many geometrical configurations, e.g.: single orifice placed at the centreline of the swirl chamber, or several off-axial orifices placed across the swirl chamber. The single axially placed orifice was found to be prone to the air-core fluctuations especially at low *SFR* regimes and produced an unstable spray. The air-core periodically decayed and were presented only within the exit orifice [6]. This behaviour was attributed to the

presence of a low-pressure zone across the SL orifice, through which the liquid can be drained from the SL to the swirl chamber and consequently fill the air-core by liquid. The off-axial SL orifices solve this problem, but their distance from the swirl chamber centreline can change the mode of liquid sheet breakup [4]. The transition from the long to short wave breakup was observed even for We_g smaller than the critical We_g. It was assumed that this phenomenon is related with fluctuations or stability of the inner air-core. This paper, among others, aims to test this hypothesis.

In the current trend with increasing efficiency of combustion, the leakage of pressure energy with the spilled liquid is inconvenient. To minimalize the energy losses, it is beneficial to connect the SL directly to the suction side of a fuel pump. However, the construction of the atomizer must prevent the air leakage to the pump suction. This was found problematic with some geometrical arrangements of the spill-return atomizers [7]. However, no relevant literature was found to deal with this problem in detail. Therefore, it will be addressed within the scope of this paper.

Experimental setup

The experiments were performed at special designed facility for cold atomizer testing at Brno University of Technology, Czech Republic.

The atomizers design

The atomizer geometry was derived from the geometry evaluated in our previous work [4]. Due to small dimensions of the original atomizers, it was impossible to manufacture them and to examine their flows directly. To solve this issue, the transparent version was designed as ten times scaled copy. The transparent atomizer has a modular construction. The assembly consist of two transparent parts made from cast polymethyl methacrylate, PMMA, which were grounded and polished to achieve transparency, and three metal parts, including exchangeable caps, see Figure 1. The operating regimes were derived from the original atomizer, as described in [6]. The Swirl number was the same for original and scaled atomizer due to design similarity, while Reynolds number, *Re*, was kept the same in order to match flow conditions.

Seven caps with different arrangement of the SL orifices were designed, see bottom part of Figure 1. For the sake of simplicity, the diameter of the SL orifices, d_s, was kept constant as d_s = 3mm. The caps C8, C11, C15 and C22 use three off-axial, parallel orifices. The orifices are placed at different distances from the swirl chamber centreline, the C8 has orifices close to the atomizer centreline at a pitch circle diameter d_{pc} = 8 mm. The C11, C15 and C22 use d_{pc} = 11, 15 and 22 mm respectively. The C8-T version is based on the C8 but contains an insert along the swirl-chamber centreline, which should reduce the air-core length and increase it stability [8]. The C8-C version is also modification of the C8 cap, but by addition of an extra orifice located at the swirl-chamber centreline. The spray instabilities are expected here. According to [6], the liquid can be drained from the SL and the air-core is to be filled by the liquid. The C14-R cap contains large insert where three spill-orifice are located and configured perpendicular to the atomizer main axis. Similarly, as for the C8-T cap, the air-core length is to be reduced here.

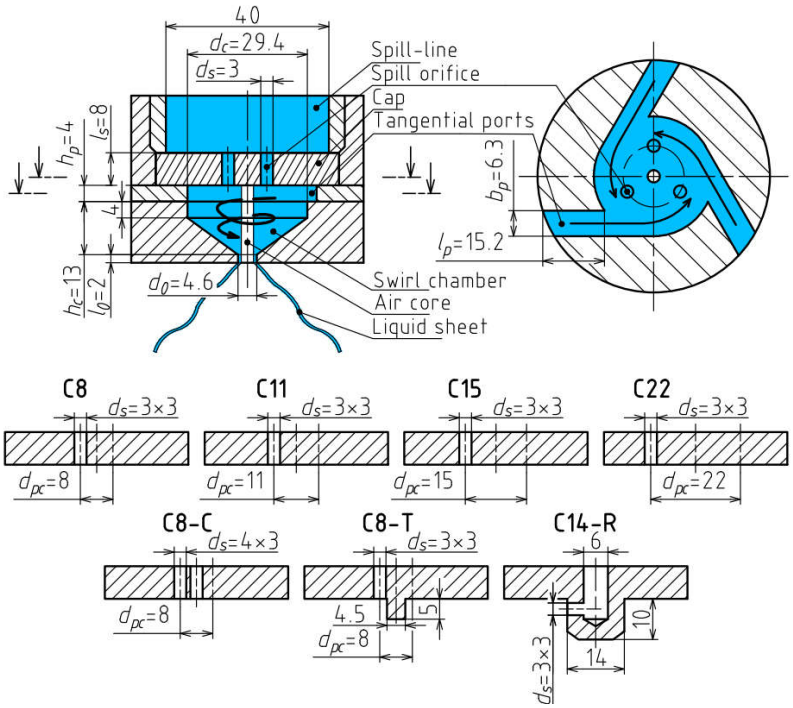

Figure 1. Top: Atomizer schematic drawing with main dimensions. Bottom: Geometry of tested caps.

The test bench

Jet A-1 fuel (Kerosene type fuel) was used as the test liquid. Physical properties of Jet A-1 at room temperature are as follows: surface tension σ = 0.029 kg/s^2, liquid dynamic viscosity μ_l = 0.0016 kg/(m·s), and liquid density ρ_l = 790 kg/m^3. The test liquid was supplied to the atomizer from a fuel tank by a centrifugal pump. The mass flow was regulated by varying the pump speed. The fuel flowing through the inlet line was metered by the Coriolis mass flow meter Mass 2100 Di3 fitted with the Mass 6000 transmitter (Siemens AG, GE) with an accuracy ±0.1% of the actual flow rate. Static inlet over-pressure was measured by a piezo-resistive pressure sensor DMP 331i (BD SENSORS s.r.o., CZ). The uncertainty in pressure sensing was 0.05 kPa. The inlet line was also equipped with a temperature sensor PR-13 made by OMEGA Engineering, INC., USA with an error of 0.2 °C. The spill-line used a piezo-resistive pressure sensor DMP 331i (BD SENSORS s.r.o., CZ), a regulation valve and a positive displacement flow meter FPD3202 with ±1% accuracy of the actual flow rate (OMEGA Engineering, Inc., USA). The calculated uncertainty of C_D was 0.25 %. The atomized liquid was captured into a collection chamber and routed back into the fuel tank. The atomizer was mounted to a CNC positioning system with a positional error less than 0.1 mm.

High-speed imaging

A FASTCAM SA-Z high-speed camera (Photron, Japan) with long-distance microscope 12X Zoom lens (NAVITAR, New York, USA) composed of 2X F-mount adapter (type 1-62922), 12 mm F.F zoom lens (type 1-50486) and attached 0.25X lens (type 1-50011) was used to document the spatial and temporal behaviour of the air-core and discharged liquid sheet. The atomizer was illuminated by a background light using an LED panel. The camera frame rate was 10,000 frames per second, the resolution was 1024 × 1024 px and the shutter speed was set to 40 µs. Mean and RMS images were calculated for each case. The air-core dimensions and the spray cone angle, *SCA*, were captured by in-house MATLAB code based on the Canny edge detector. There were four locations, each with different axial distance, where the air-core diameter and its surface waves and fluctuations were evaluated, see Figure 2. Similarly, two locations were evaluated for the liquid sheet cone fluctuations. The temporal fluctuations and waves were processed using Fast Fourier Transform, FFT.

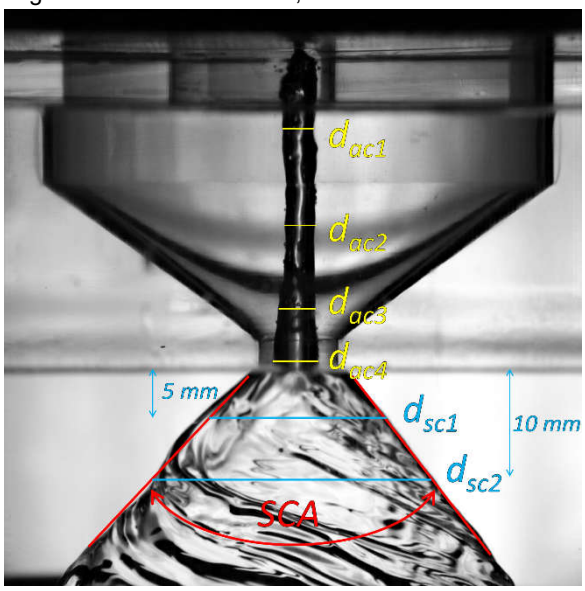

Figure 2. The typical result from the high-speed visualization with measured positions

Results and discussion

Results are divided into four parts. The first part is focused on the discharge parameters of the atomizers. The second one deals with spray cone angle and spray stability. The third focus on the internal air-core characteristics, while the fourth compare the temporal characteristics of the air-core and liquid sheet for the C8 and C15 atomizers.

Discharge characteristics

The discharge parameters were measured at p_l = 5 kPa and for several *SFR* regimes in a range from a closed spill line to fully open. All the atomizers, except C8-C, yield an identical flow rate for *SFR* = 0 of $\dot{m}_{inj}$ = 77.5 ± 1 kg/h, which outcomes into a discharge coefficient of C_D = 0.46 ± 0.01. This is in fair agreement with prediction by Rizk [9], where C_D = 0.42. The C8-C atomizer produces an unstable spray with $\dot{m}_{inj}$ = 100 kg/h for *SFR* = 0, which results in C_D = 0.58. This was expected, since no stable air-core is developed in this regime (see following chapters) and the flow cross-section of the exit orifice is therefore larger. When the spill-line is open, the atomizers differs. The $\dot{m}_s$ and $\dot{m}_{inj}$ are plotted for each atomizer for *SFR* = 0.6 in Figure 3, left. It is evident, that the overall liquid consumption grows with increasing d_{pc}. This trend was predicted in our previous work, where also the differences among the

atomizers raises with *SFR* [4]. The C8 and C8-T atomizers feature both the lowest $\dot{m}_s$ and $\dot{m}_{inj}$. Thus, they can be attributed as to the most spill-efficient. On the other hand, the C8-C consume the highest amount of the liquid which is in contrast to the single axially placed orifice, which achieved the highest turn-down capability in [4]. The inserts into the swirl chamber in the case of C8-T and C14-R atomizers have no effect on the flow-rates for all tested regimes.

As long as the $\dot{m}_{inj}$ change with the used atomizer, the turn-down ratio likewise differs, see right part of Figure 3, where the turn-down ratio is calculated as a ratio of $\dot{m}_{inj}$ for *SFR* = 0 to $\dot{m}_{inj}$ for *SFR* = 0.6. Note that all the atomizers with d_{pc} = 8 mm achieved identical turn-down ratio of 2.05, even the C8-C version which flow rates are higher by 25 % compared to the C8 atomizer for all investigated *SFR*s.

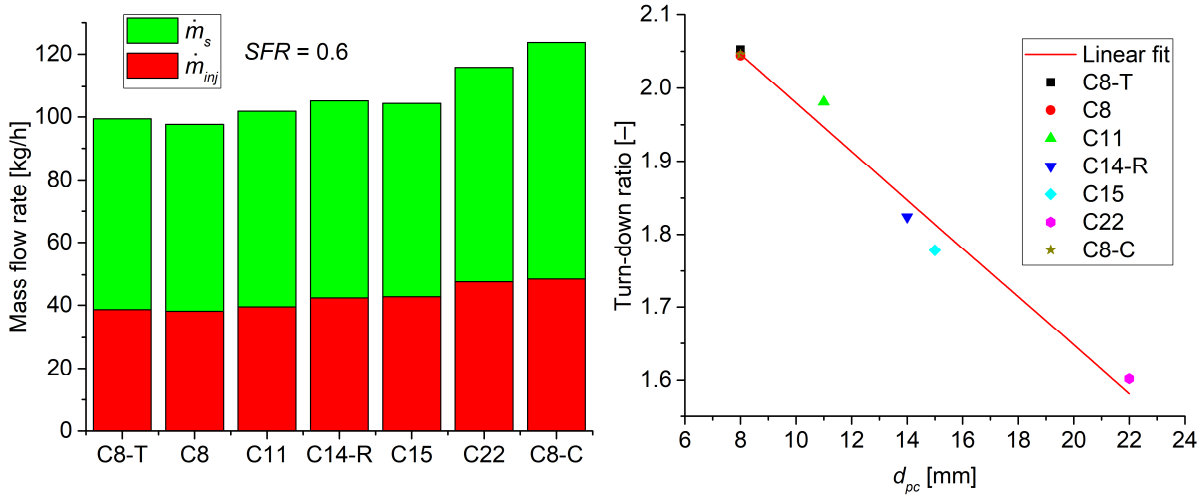

Figure 3. Mass flow rates (left) and turn-down ratio (right) for p_l = 5 kPa and *SFR* = 0.6.

Spray cone angle and stability

Since the only geometrical variation among tested atomizers is the position of the SL orifices, the change in the *SCA* is only possible through a change of the swirl to axial momentum ratio, which changes with *SFR*. This phenomenon was addressed in several papers [4, 10, 11]. In our recent paper [4], an empirical correlation of the *SCA* and *SFR* was proposed as:

$$SCA = Bp_l^{0.1}(1 - SFR)^{-0.15} \quad (1)$$

where *B* is an empirical constant related to the atomizer geometry and the rheology of the liquid used. In this case, *B* = 32. The fit is shown in Figure 4, the unstable C8-C atomizer is excluded from the fit. The *SCA* is literally equal for all the atomizers expect the C8-C for *SFR* = 0 and 0.3. The differences among the atomizers rises at *SFR* = 0.6 and higher. The spray stability was evaluated using a standard mean deviation of the *SCA*. The C8-C reach the standard mean deviation about 10°, which corresponds to a significantly fluctuating spray. The standard mean deviation is weakly dependent on the d_{pc}, since the C8 atomizer reaches 3.5° and it decreases to 2.5° for the C15 and C22 atomizers for *SFR* = 0. However, for *SFR* ≥ 0.6, the spray fluctuations grow about 60 % for all the atomizers.

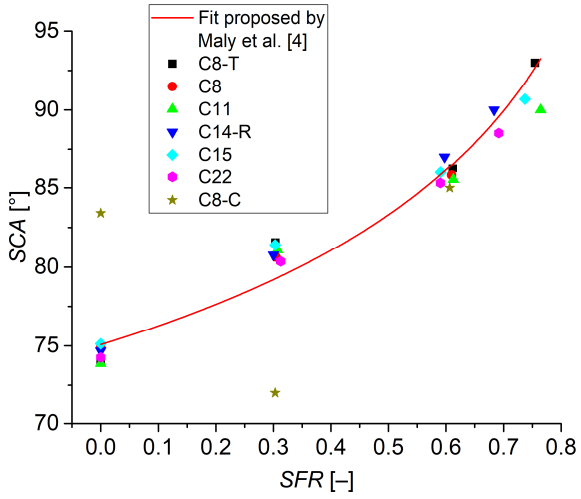

Figure 4. The *SCA* in dependency on *SFR*.

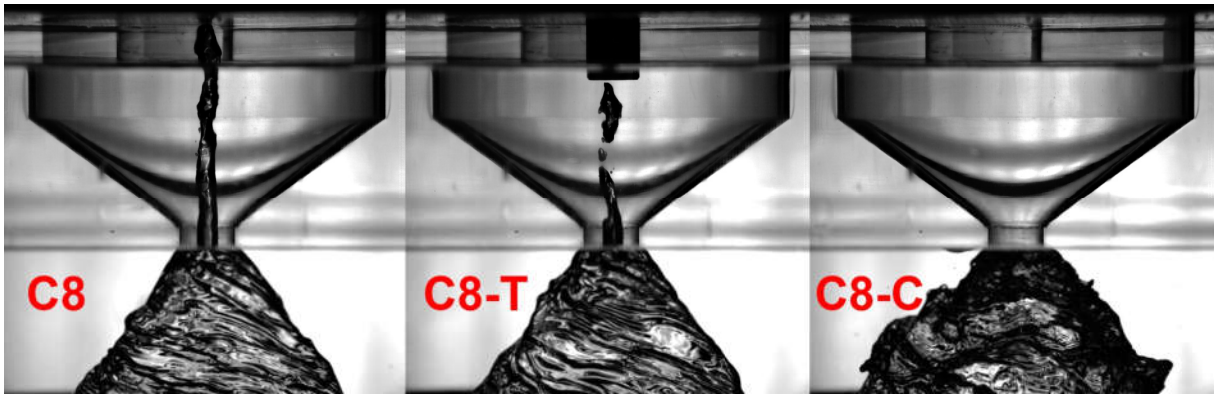

Figure 5. Comparison of the air-core behaviour of the C8, C8-T and C8-C atomizers for *SFR* = 0.

Internal air-core and liquid sheet

The fluctuations of the spray cone are typically related with the liquid sheet stability prior discharge which is linked with the air-core stability that can be depend on the geometry of the SL orifice. This is clearly evident in the case of C8-C, where the air-core is not developed and its length never exceeds the exit orifice length, even for *SFR* = 0.6 – see Figure 5. The phenomenon of non-existing air-core was studied in detail in [6]. In all other cases, the air-core is developed across the whole swirl chamber. The slight exception can be found in the case of C8-T atomizer at *SFR* = 0, where the air-core occasionally splits into several parts, as it is shown in Figure 5. This result was unexpected since the shorter swirl chamber should rather stabilize the air-core as described in [8]. Nevertheless, the dimensions and stability of the air-core within the exit orifice, d_{ac4}, are equal with the C8 version. This is well evident in Figure 6 left where the air-core dimensions of d_{ac2} and d_{ac4} are plotted in dependency on *SFR*. Note that the greatest differences between the atomizers can be found for d_{ac2} at *SFR* = 0. These differences almost diminish inside the exit orifice; see small variations of d_{ac4}. The air-core is greater in diameter inside the exit orifice, which is well know phenomenon [12, 13]. With increasing *SFR*, the difference between d_{ac2} and d_{ac4} is decreasing and both the air-core diameters are linearly increasing with *SFR* due to rising liquid flow rate through the tangential ports which outcomes into a stronger swirl motion.

The air-core was found to not penetrate through the SL orifice and also no air leakage inside the SL line was detected for all the atomizers and *SFR*s. However, the SL orifice located at the swirl chamber centre line allows the air-core to enter the SL and consequently feed air into the pump suction.

The liquid sheet thickness, *t*, is one of the crucial parameters to predetermine droplet sizes and breakup mode [3]. It could be easily calculated if d_{ac4} is known. However, if no direct measurement of d_{ac4} is performed, it could be calculated from continuity equation as:

$$\dot{m}_{inj} = \pi \rho_l U_l t (d_o - t), \tag{2}$$

where U_l is an axial velocity inside the exit orifice. Determination of U_l is the crucial aspect here. For practical applications, it is convenient to approximate the U_l from the axial velocity of the discharged liquid sheet, which can be easily measured using e.g. PIVlab® on high-speed records or Laser Doppler Anemometry, LDA. The relationship between the PIVlab® and LDA results was discussed in [4], where the both approaches were found to be reliable and differs each other less than 2%. The correlation between measured and calculated values of *t* is shown in Figure 6, right. The error bars correspond to the measurement repeatability error. The calculated values of *t* are shifted from the measured values of *t* about 0.28 mm. The indirect approach overestimates the mean axial velocity within the exit orifice since it neglected the presence of boundary layer. Further research need to be conducted.

Since the air-core generally fluctuates in its diameter or position, the discharged liquid sheet can be affected by means of surface waves. The initial frequency and amplitude of surface waves are linked with the air-core fluctuations, which depends on the internal geometry and operating conditions. Temporal surface wave oscillations can be obtained by fixing a location and observing the wave change as a function of time. In this way, spatiotemporal diagrams of the liquid sheet and air-core were obtained, where each vertical line corresponds to a fixed line from the high-speed images at different time.

As the surface wave propagates downstream, its amplitude increases, but the frequency remains the same, see the spatiotemporal diagram of the liquid sheet in Figure 7, which was taken at two different downstream positions, where blue is for d_{sc2} and black for d_{sc1}. However, no dominant frequency or wave mode is observable here and also FFT did not reveal any dominant waves. Similarly, rather random waves are observed for rest atomizers and regimes. A comprehensive study of liquid sheet waves were performed in the past [14], where the dominant wave frequency was obtainable only for relatively high-viscous liquids, which confirms our findings. As the amplitude of the surface wave reaches a critical value, the liquid sheet breaks up into ligaments. Since the breakup length is out of the visualized area here, the breakup nature can be discussed only indirectly, as it is in the following chapter.

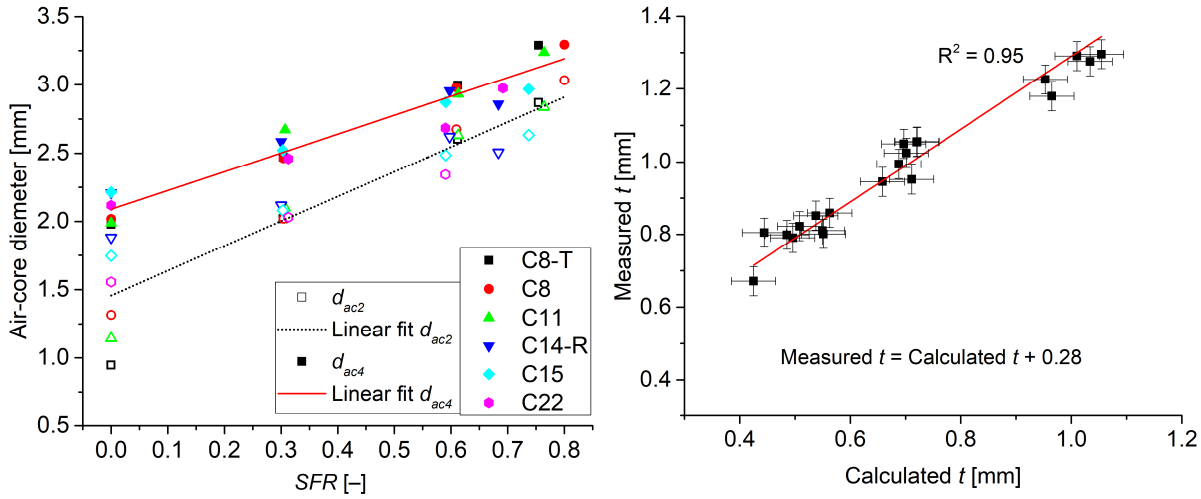

Figure 6. Left: The air-core dimensions d_{ac2} and d_{ac4}. Right: Comparison of the measured and calculated t from eq. 2.

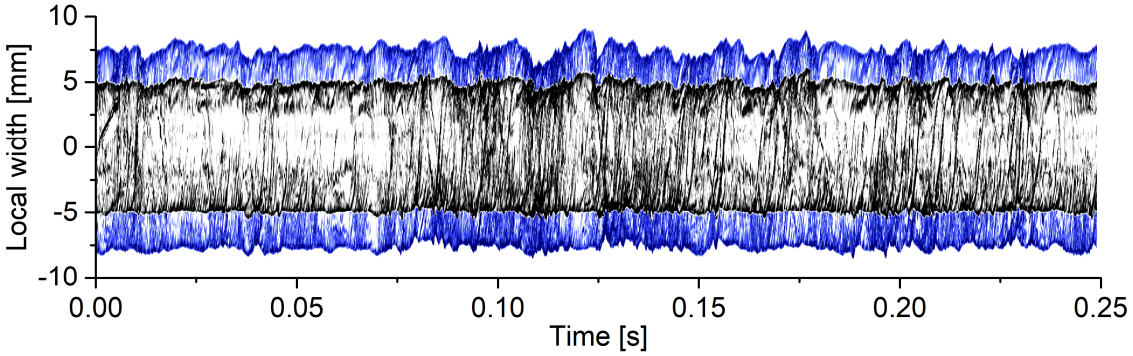

Figure 7. The temporal evolution of the liquid sheet surface waves for the C8 atomizer and *SFR* = 0.3.

Comparison of liquid sheet and air-core stability from the C8 and C15 atomizer

In our recent paper [4], two different modes of liquid sheet breakup, the short and long wave breakup mode, were recognised for identical operating conditions but different SL orifice geometry. This change in the breakup mode was attributed to the differences in the internal flow, respectively to the change in the initial frequency and amplitude of the liquid sheet surface waves. Therefore, this subchapter is focused on the liquid sheet and air-core behaviour of the C8 and C15 atomizers, which have the similar SL orifice design as investigated in [4]. The scaled atomizer used here ensures similar conditions of the internal flow [6] and are tested at the same *SFR*s, but the We_g, which is responsible for liquid breakup nature, reaches values of We_g = 0.12 to 0.05 in dependency on *SFR*. These values are roughly ten times lower than investigated in [4]. Since the We_g is much lower than critical value of 27/16, the long wave breakup more likely occurs for each operating regime. Despite different We_g, the air-core fluctuations and initial surface waves should be analogous to the original atomizers.

Since both the atomizers achieved the identical flow-rates and mean air-core diameters, a temporal evaluation has to be conducted. In top part of Figure 8, spatiotemporal diagrams of the liquid sheet waves taken at d_{sc2} and the temporal fluctuations of the air-core are presented. At these points, the FFT was also processed, see Figure 9. It is seen that the liquid surface waves can be well observed, but the liquid sheet has rather random nature of wave propagation, since no dominant frequency is to be found for either atomizer. However, there are small differences in the liquid sheet surface structure. The high-frequency waves are presented there in the case of C8 atomizer, and they are also detectable by the FFT, see the frequency range of 600-800 Hz. These waves are insignificant in the case of C15 atomizer, which performed much smoother liquid sheet surface. The high-frequency waves may be responsible for the short-wave breakup mode, which was observed in [4] for the atomizer with similar design to the C8. The observed liquid sheet waves have to be linked with the air-core fluctuations. The air-core is fully developed and cylindrical for both cases, but it fluctuates in diameter within the swirl-chamber, see bottom part of Figure 8. These fluctuations are subdued inside the exit orifice due to stronger swirl motion there. Nevertheless, the FFT of the air-core fluctuations within the exit orifice reveals much higher FFT magnitudes for the C8 atomizer for frequencies up to 1 kHz. Though, no significant frequency peak was found. Note, that the air-core surface at given time step is very smooth – see Figure 5, but its shape is rapidly changing in the temporal domain. Since the air-core is not perfectly cylindrical, it slight change its diameter and position during each revolution and due to camera frame-rate, a sharp change in the temporal domain can occurs.

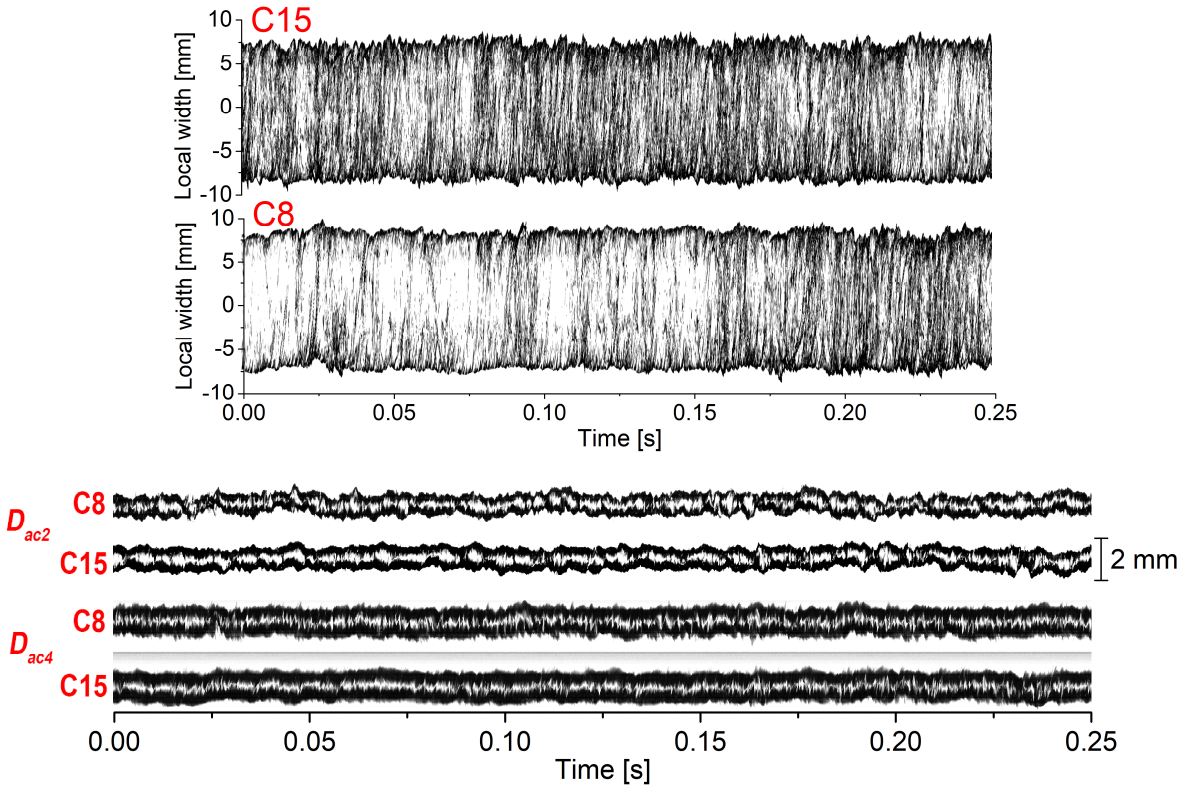

Figure 8. Spatiotemporal diagrams. Top: Comparison of surface waves on the liquid sheet of C8 and C15 atomizer for *SFR* = 0, d_{sc2}. Bottom: Temporal stability of the air-core.

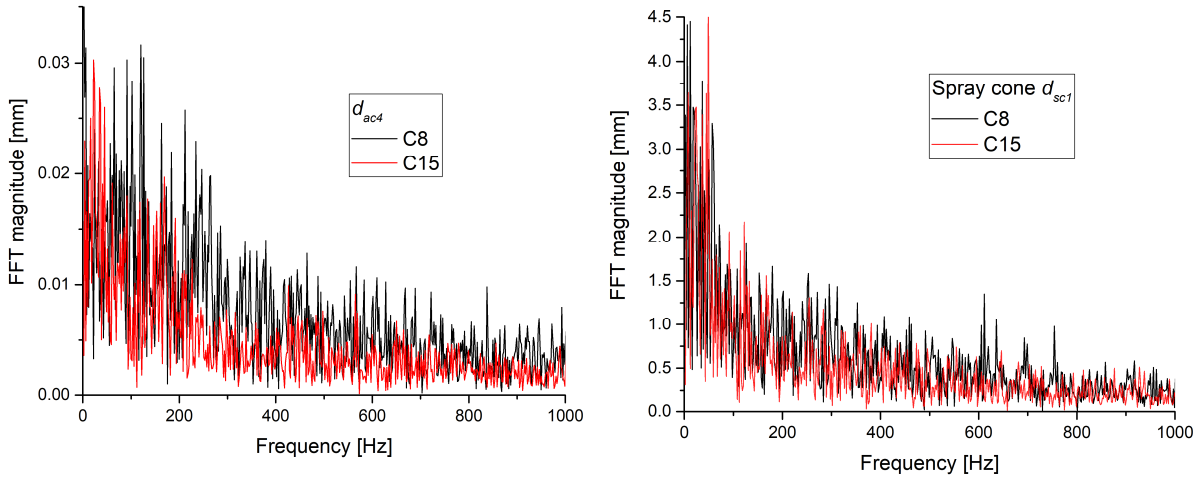

Figure 9. FFT of the air-core surface at the position of d_{ac4} (left) and liquid sheet at d_{sc1} (right) fluctuations

Conclusions

Experimental investigation of seven transparent spill-return atomizers was performed using high-speed imaging. The turn-down ratio was found to be affected by the pitch circle diameter, d_{pc}, on which the spill-line (SL) orifices are located. An increase in d_{pc} reduces the turn-down capability.

The spray cone was found to be stable for all atomizers, except the C8-C, which has a combination of single central and three off-axial SL orifices. This atomizer produces no air-core inside the swirl-chamber. The air-core is presented there only for spill-to-feed ratio, *SFR* > 0.6, and it is limited only inside the exit orifice. The cylindrically shaped air-core, wider in diameter within the exit orifice, was found for the other atomizers. The air-core diameter is linearly increasing with *SFR* and difference between its diameter inside the swirl chamber and exit orifice decrease with *SFR*.

The measured liquid sheet thickness, *t*, was compared with the calculation based on the Continuity equation but using the axial velocity of the discharged liquid sheet instead of the axial velocity of the liquid sheet within the exit orifice. The correlation between measured and calculated values of *t* proved, that *t* can be estimated without necessity of using transparent atomizer.

The temporal characteristics of the air-core and discharged liquid sheet were examined in detail for the C8 and C15 atomizers. High-frequency waves were found for the C8 atomizer; however, their amplitudes were small. The FFT did not reveal any dominant frequency, neither for air-core or liquid sheet, but showed slightly higher magnitudes of air-core fluctuations for the C8 atomizer. The high-frequency waves may cause change of the liquid sheet breakup mode, which was described in [4].

Acknowledgements
The authors acknowledge the financial support from the project No. 18-15839S funded by the Czech Science Foundation and the project “Computer Simulations for Effective Low-Emission Energy” funded as project No. CZ.02.1.01/0.0/0.0/16_026/0008392 by Operational Programme Research, Development and Education, Priority axis 1: Strengthening capacity for high-quality research.

Nomenclature

A	area [m^2]
b	width [m]
C_D	discharge coefficient [–]
d	diameter [m]
d_{pc}	Pitch Circle Diameter [m]
h	height [m]
l_b	breakup length [m]
$\dot{m}$	mass flow rate [kg/h]
r	radial distance [m]
Re	Reynolds number [–]
SCA	spray cone angle [°]
SFR	Spill-to-Feed ratio [–]
t	liquid sheet thickness [m]
U	axial velocity
We_g	gas Weber number [–]
Z	axial distance [m]

Greek characters

p	pressure drop at the nozzle [Pa]
μ	dynamic viscosity [kg/(m·s)]
ρ	density [kg/m^3]
v	kinematic viscosity [m^2/s]
σ	liquid/gas surface tension [kg/s^2]

Subscripts and Superscripts

c	swirl chamber
g	surrounding gas
inj	injected
l	atomized liquid
p	inlet port
s	spill-line
ac	air-core
sc	spray cone

References

[1] Lefebvre, A. H., and McDonell, V. G., 2017, Atomization and sprays, CRC press.
[2] Chinn, J., Cooper, D., Yule, A., and Nasr, G., 2015, "Stationary rotary force waves on the liquid–air core interface of a swirl atomizer," Heat and Mass Transfer, pp. 1-14.
[3] Fu, Q.-F., Yang, L.-J., Qu, Y.-Y., and Gu, B., 2010, "Linear Stability Analysis of a Conical Liquid Sheet," Journal of Propulsion and Power, 26(5), pp. 955-968.
[4] Maly, M., Sapik, M., Cejpek, O., Wigley, G., Katolicky, J., and Jedelsky, J., 2019, "Effect of spill orifice geometry on spray and control characteristics of spill-return pressure-swirl atomizers," Experimental Thermal and Fluid Science, Accepted manuscript.
[5] Senecal, P. K., Schmidt, D. P., Nouar, I., Rutland, C. J., Reitz, R. D., and Corradini, M. L., 1999, "Modeling high-speed viscous liquid sheet atomization," 25(6), pp. 1073-1097.
[6] Maly, M., Jedelsky, J., Slama, J., Janackova, L., Sapik, M., Wigley, G., and Jicha, M., 2018, "Internal flow and air core dynamics in Simplex and Spill-return pressure-swirl atomizers," International Journal of Heat and Mass Transfer, 123, pp. 805-814.
[7] Carey, F. H., 1954, "The Development of the Spill Flow Burner and Its Control Systemfor Gas Turbine Engines," Journal of the Royal Aeronautical Society, 58, pp. 737-753.
[8] Kim, S., Khil, T., Kim, D., and Yoon, Y., 2009, "Effect of geometric parameters on the liquid film thickness and air core formation in a swirl injector," Measurement Science and Technology, 20(1).
[9] Rizk, N. K., and Lefebvre, A. H., 1985, "Internal flow characteristics of simplex swirl atomizers," Journal of Propulsion and Power, 1(3), pp. 193-199.
[10] Rizk, N. K., and Lefebvre, A. H., 1985, "Spray characteristics of spill-return atomizers," Journal of Propulsion and Power, 1(3), pp. 200-204.
[11] Nasr, G., Yule, A., Stewart, J., Whitehead, A., and Hughes, T., 2011, "A new fine spray, low flowrate, spill-return swirl atomizer," Proceedings of the Institution of Mechanical Engineers, Part C: Journal of Mechanical Engineering Science, 225(4), pp. 897-908.
[12] Halder, M., Dash, S., and Som, S., 2002, "Initiation of air core in a simplex nozzle and the effects of operating and geometrical parameters on its shape and size," Experimental thermal and fluid science, 26(8), pp. 871-878.
[13] Amini, G., 2016, "Liquid flow in a simplex swirl nozzle," International Journal of Multiphase Flow, 79, pp. 225-235.
[14] Yao, S., Zhang, J., and Fang, T., 2012, "Effect of viscosities on structure and instability of sprays from a swirl atomizer," Experimental Thermal and Fluid Science, 39, pp. 158-166.